Petroleum Science 23 (2026) 1053–1065

Contents lists available at ScienceDirect

Petroleum Science

journal homepage: www.keaipublishing.com/en/journals/petroleum-science

Original Paper

Assessment of shale hydrocarbon evaporative loss during exposure: Insights from online low-field nuclear magnetic resonance observations in the Qingshankou Formation, Songliao Basin, China

Xue-Ning Qi [a,b], Hua Tian [a,b], Xiao-Mei Wang [a,b,*], Ming-Hao Wu [a,b], Yu-Ke Liu [a,b], Shui-Chang Zhang [a,b]

[a] Research Institute of Petroleum Exploration and Development, PetroChina, Beijing, 100083, China
[b] Key Laboratory of Petroleum Geochemistry, China National Petroleum Corporation, Beijing, 100083, China

ARTICLE INFO

Article history:
Received 19 January 2025
Received in revised form
9 May 2025
Accepted 11 September 2025
Available online 17 September 2025

Edited by Xi Zhang and Jie Hao

Keywords:
Evaporative hydrocarbon loss
Shale oil
Songliao Basin
Low-field nuclear magnetic resonance
Qingshankou Formation

ABSTRACT

Understanding the evaporative loss of shale oil is critical for the shale oil resources assessment. However, previous studies have largely neglected the rapid evaporative loss of shale oil that occurs immediately after drill cores are retrieved to the surface at the well site. Thus, the factors influencing the evaporative loss of shale oil during thermal evolution remain inadequately explored. In this study, closed-system pyrolysis experiments were carried out to the artificially mature Qingshankou Formation shales. Subsequently, low-field nuclear magnetic resonance (LF-NMR) techniques were utilized to monitor the variations in oil content of the shales under different exposure times. Our experimental approach successfully reconstructed the entire evaporative loss process of shale oil, spanning from its original subsurface location to the well site, from the well site to the laboratory, and ultimately to long-term core storage. We find that the maximum loss of shale oil reaches approximately 10% within the first 10 h following the retrieval of drill cores from the subsurface to the ground, followed by a gradual deceleration, and the maximum loss ranges from 11% to 89%. As thermal maturity increases to a range of R_o = 0.89%–1.20%, the loss proportion of shale oil shows a decreasing trend, which can be attributed to the reduction in total organic carbon (TOC) content. It is worth mentioning that the loss proportion of shale oil exhibits a continuous increasing trend at the thermal range of 1.20%–1.75%. At this stage, the hydrocarbon composition (C_6–C_{14}/C_{15+} ratio) may be the mainly controlling factors for the shale oil loss proportion, while TOC content and nanopore volume serve as secondary factors. Our analyses reveal that hydrocarbon evaporative loss of shale oil is complex and involves various factors, especially the first 10 h during the transfer of the shale from its in-situ reservoir to the surface at the well site, which is critical to the understanding of shale oil occurrence and accurate resource assessment.

1. Introduction

Shale oil is an important global energy resource (Hughes, 2013; Hopkins, 2017; Hong et al., 2025). However, inaccurate estimates of the initial total content of shale oil can lead to erroneous assessments of shale oil resources (Abrams et al., 2017; Wang et al., 2022). Especially, the evaporative hydrocarbon loss of shale oil is often ignored during the evaluation of the total oil content of shale (Jarvie, 2012; Michael et al., 2013; Jiang et al., 2016; Hu et al., 2021; Wang et al., 2022).

Previous studies have investigated evaporative loss of shale oil from the well site to the laboratory or during the storage of core samples at ambient conditions in different regions (Song et al., 2013; Zhu et al., 2015; Jiang et al., 2016; Chen et al., 2017, 2018; Sun, 2020; Zhao et al., 2023). While the previous studies have generally overlooked the evaporative loss of hydrocarbons during drilling and core recovery to the surface at the well site, there might be an enormous loss of hydrocarbons caused by changes in temperature and pressure during this process (Jarvie, 2012).

The studies from the well site to the laboratory or during the storage of core samples have been carried out in different basins,

* Corresponding author.
E-mail address: wxm01@petrochina.com.cn (X.-M. Wang).
Peer review under the responsibility of China University of Petroleum (Beijing).

https://doi.org/10.1016/j.petsci.2025.09.024

For example, in the Bohai Bay Basin in China, the shale oil loss in the Paleogene Shahejie Formation varies in different depressions, with reported losses of 9%–52% of the storage of core samples at ambient conditions in the Jiyang Depression (Song et al., 2013; Chen et al., 2017). The Dongying Depression contains shale with total organic carbon (TOC) contents ranging from 1.4 wt% to 8.7 wt% (mostly 2.0–4.0 wt%; with an average of 3.1 wt%) that underwent shale oil loss of 5.23%–25.65% after 30 days of storage under ambient conditions (Zhu et al., 2015). The Damintun Sag contains shale with TOC contents of 0.47–14.0 wt% (mean = 6.45 wt%) that exhibited shale oil maximum loss proportion of 37.5%–47.4% (Chen et al., 2017). Shale samples from other basins exhibit varying degrees of hydrocarbon loss under ambient conditions. A core sample of organic-rich shale (TOC = 11.90 wt%) from the Devonian Duvernay Formation in the Western Canada Sedimentary Basin stored for 2 years lost 15% of its oil content after 360 h exposed to open air, increasing to 22.5% after 1300 h. An organic-poor shale (TOC = 0.86 wt%) from the Ordovician Lotbinière Formation in the St. Lawrence Platform, Quebec, Canada kept at ambient conditions for 6 months, showed 15% hydrocarbon evaporative loss after 21 h and 29% after 170 h after being exposed to open air (Jiang et al., 2016). In the Junggar Basin, shale samples from the Lucaogou and Fengcheng formations (TOC = 1.03–12.31 wt%, mean = 5.09 wt%) exhibited hydrocarbon losses of 11%–89% after being stored at ambient conditions (Chen et al., 2018). In the Songliao Basin, the hydrocarbon loss was 70% when comparing core samples with those stored under high-pressure conditions (Sun et al., 2020). In the Qaidam Basin, shale from the Ganchaigou Formation experienced hydrocarbon loss of 43% after 43 h of exposure (Zhao et al., 2023). So, the above study focuses on hydrocarbon loss of samples from the well site to the laboratory, the long-term storage of core samples, and sample preparation.

Therefore, we divide the hydrocarbon loss from the recovery of drillcore to final analysis into three stages, stage 1 occurs during the transfer of the shale from its in-situ reservoir to the surface at the well site, which takes about 10 h (Yan et al., 2019). Stage 2 occurs during the transportation of the shale from the well site to the laboratory, which includes core sorting, packaging, and transport. The transportation time depends on the location of the well site (Zhu et al., 2015; Luo et al., 2022), but it is generally ~150 h. Stage 3 occurs during the storage of core samples, with some samples being analyzed promptly, while others are placed in long-term storage (e.g., > 1000 h) until needed (Jiang et al., 2016).

And the previous studies have investigated three key factors controlling shale oil loss: thermal maturity, TOC content, and pore diameter (Song et al., 2013; Zhu et al., 2015; Jiang et al., 2016; Chen et al., 2017, 2018). While they have different opinions about the relationship between thermal maturity (expressed as vitrinite reflectance, R_o) and hydrocarbon loss at different mature stage, during the maturity range of R_o = 0.5%–0.7%, the hydrocarbon loss remains constant (Zhu et al., 2015); the hydrocarbon loss may increase (Song et al., 2013; Zhu et al., 2015) or decrease (Chen et al., 2017, 2018) with increasing maturity at the maturity range of R_o = 0.7%–1.2%; and when over the maturity range of R_o = 1.3%–1.6%, the hydrocarbon loss increases with increasing maturity (Chen et al., 2017, 2018).

The effect of TOC content on shale oil loss is also controversial. Organic-rich shale has a stronger ability to retain oil and gas due to its hydrocarbon adsorption, and thus tends to retain more oil and gas, leading to lower hydrocarbon loss (Jiang et al., 2016; Yan, 2023). However, other studies have suggested that hydrocarbon loss increases at higher TOC contents (Chen et al., 2018). In terms of hydrocarbon composition during evaporative loss, it has been qualitatively observed that lighter components are more prone to hydrocarbon loss than heavier components (Michael et al., 2013; Jarvie et al., 2007; Jiang et al., 2016; Şen and Kozlu, 2020; Sun, 2020).

Some studies have suggested that heavier hydrocarbon components are also susceptible to loss (e.g., Tian et al., 2024). But few studies have quantitatively examined how differences in hydrocarbon composition or carbon numbers affect hydrocarbon loss. Some other studies have highlighted the influence of nanopores during thermal evolution on shale oil loss (Milliken et al., 2013; Zou et al., 2013). When the pore size is below a certain threshold, smaller molecular weight hydrocarbons can be trapped in nanopores (Akkutlu, 2017). An increase in hydrocarbon generation due to the decomposition and transformation of kerogen during hydrocarbon generation leads to an increased nanopore volume (Curtis et al., 2012; Milliken et al., 2013), resulting in more adsorbed hydrocarbons and reduced hydrocarbon loss (Jiang et al., 2016; Chen et al., 2018).

Although the previous studies have investigated shale oil evaporative loss, establishing preliminary insights into controlling factors of this loss (Song et al., 2013; Zhu et al., 2015; Jiang et al., 2016; Chen et al., 2018), there are three key problems still unclear. First, the proportion and rate of hydrocarbon loss during stages 1 and 2 have not been thoroughly investigated. Second, the factors that affect shale oil loss are unclear. Third, there is some controversy regarding the loss of light and heavy hydrocarbon components, and there has been no quantitative study on the relationship between hydrocarbon composition and proportion of hydrocarbon loss from shale.

This study conducted detailed analyses of geochemical characteristics of the simulated shale samples, monitoring the proportion and rate of shale oil loss over varying exposure times. Furthermore, the research identified key factors that control evaporative hydrocarbon loss factors across different thermal maturity stages. These findings highlight the importance of timely analysis of shale samples and provide guidance for the accurate evaluation of shale oil and gas resources.

2. Materials and methods

2.1. Samples

The original samples were obtained from the Upper Cretaceous Qingshankou Formation within the Sanzhao Sag, which represents one of the secondary tectonic units within the Central Depression of the Songliao Basin (Fig. 1).

The geochemical characteristics of the samples are presented in Table 1. Based on the geochemical parameters, the samples have a low maturity and high hydrocarbon generation potential.

2.2. Methods

The shale samples were prepared by removing weathered surfaces, washing with deionized water, and drying in a vacuum oven at 80 °C. The samples were then crushed to 60–80 mesh, and 100 g aliquots were prepared using the quartering method.

The thermal simulation experiments were conducted under the same room temperature and pressure conditions to obtain artificially matured shale samples with R_o = 0.89%–1.75%. A small amount (100 mg) of each artificial matured sample was used for determination of TOC contents, and 15 g of each sample was subjected to online continuous LF-NMR T_2 spectral analysis. About 1 g of each sample was used for low-temperature N_2 adsorption experiments and approximately 20 g of each sample was subjected to Soxhlet extraction to obtain a solid residue that did not contain shale oil. After extraction, extractable organic matter (EOM) was

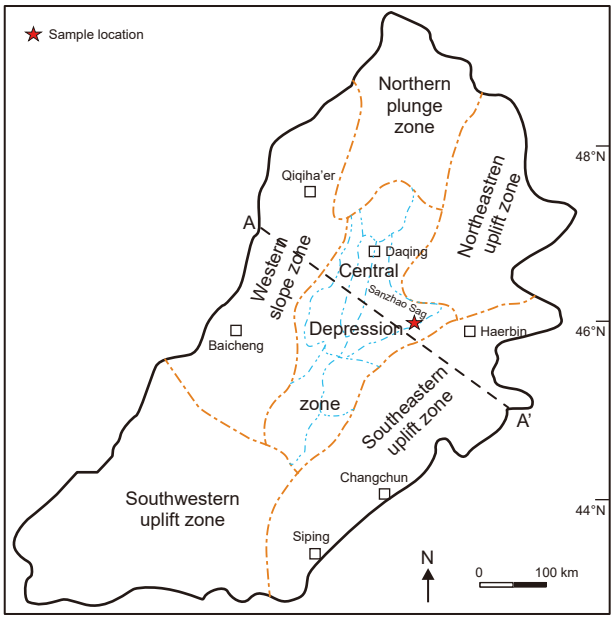

Fig. 1. The location of original samples in this study (Modified from Tian et al., 2023).

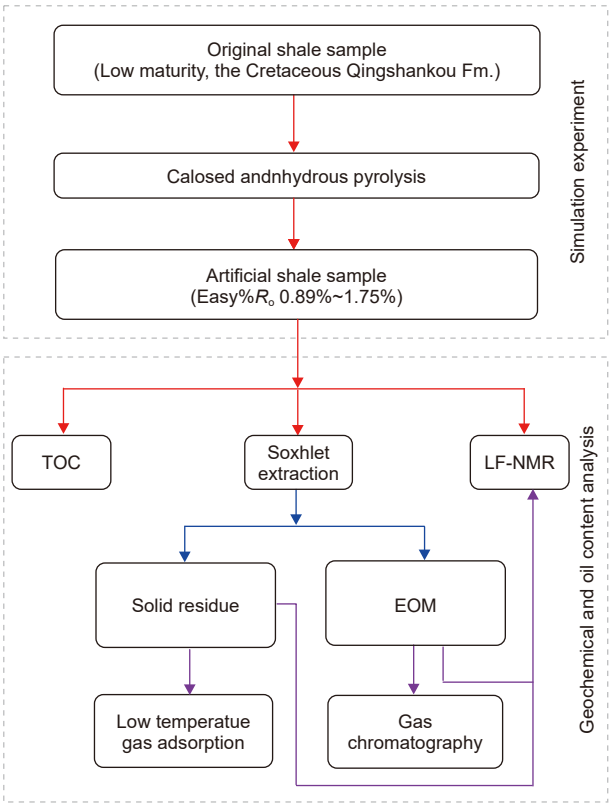

Fig. 2. Experimental workflow for the comprehensive assessment of hydrocarbon evaporative loss of shale samples Fm. = Formation.

Table 1
Geochemical parameters of the Qingshankou Formation shale samples.

Well	Depth, m	TOC, %	S_1, mg/g	S_2, mg/g	S_3, mg/g	T_{max}, °C	HI, mg/g TOC	R_o, %
X	805	4.87	0.82	42.84	0.33	440	879	0.70

obtained for gas chromatography (GC) analysis and the LF-NMR experiments. About 10 g of solid residue was dried in a vacuum oven at 80 °C for 24 h to remove dichloromethane and the dried sample was then subjected to LF-NMR analysis. This study used LF-NMR to continuously monitor the changes in the LF-NMR signal of different shale samples over time, recording the decrease in shale oil content and providing real-time insights into the evaporative loss of hydrocarbons. The experimental process is shown in Fig. 2.

2.2.1. Pyrolysis simulation experiments

The thermal simulation experiments used a water-free closed system to minimize external H contamination. Before the thermal simulation experiments, shale samples (100 g) were dried at 80 °C for 24 h in a vacuum oven to remove moisture. The dried samples were transferred to a stainless-steel tube and sealed with a graphite gasket. The tube was loaded into a high-pressure pyrolysis apparatus developed by the China Petroleum Exploration and Development Research Institute (Mi et al., 2009). A closed system was utilized in this study to replicate subsurface geological conditions. Typically, a 100 g sample was placed in a stainless-steel cylinder (inner diameter: 34 mm), and an axial pressure of 80 MPa was applied from one end of the cylinder to compact the sample.

The burial depth during the simulation was set to 2500 m, with pyrolysis temperatures ranging from 330 °C to 420 °C over a duration of 2–8 days. The R_o values were calculated using the method of Sweeney and Burnham (1990). The equivalent R_o values for the experimental temperatures and heating durations are presented in Table 2. The thermal simulation experiment produced shale samples with a maturity of R_o = 0.89%–1.75%, the main generation stage for shale oil. These samples were subsequently subjected to LF-NMR analysis, where the proportion and rate of shale oil loss were continuously monitored in real-time over varying periods under ambient conditions.

Table 2
Experimental temperatures (°C) and heating time (days) corresponding to equivalent R_o values (Easy%R_o).

Sample	Temperature, °C	Time, days	Easy%R_o
1	330	3	0.89
2	330	4	0.92
3	350	2	1.02
4	350	4	1.13
5	350	6	1.20
6	380	2	1.37
7	380	3	1.45
8	380	5	1.56
9	400	2	1.65
10	400	3	1.75

Note: "Temperature" is the temperature of the kettle after 2 h of heating from room temperature, which is maintained at constant temperature during the experimental process. "Time" is the thermal reaction time of the original sample in the reactor under the specified temperature. "Easy%R_o" is calculated using the method described by Sweeney and Burnham (1990).

2.2.2. LF-NMR analysis

The first LF-NMR spectrum for each shale sample was acquired approximately 30 min after completing the thermal simulation experiment, with subsequent data acquisition every 2 min interval during the first hour. As the rate of signal change slowed, the data acquisition interval was increased to 22 min. The LF-NMR settings were programmed for automatic data acquisition, which continued for 5 days. The longest data-acquisition time for the shale samples exceeded 1000 h.

The LF-NMR analyses were conducted with a MacroMR12-110H-G system (Niumag, China), with a magnetic field strength of 0.3 T, probe coil diameter of 25 mm, resonance frequency of 12 MHz, sampling frequency of 333.33 kHz, and magnet temperature of 32 °C. The transverse relaxation time (T_2) spectra were acquired using the Carr-Purcell-Meiboom-Gill (CPMG) pulse sequence (Tian et al., 2024), with analytical parameters as follows: echo time interval = 0.1 ms, wait time = 2000 ms, number of echoes = 8000, and number of scans = 32. Before conducting the LF-NMR analyses for each sample, the instrument was calibrated using the Flame Ionization Decay sequence to optimize frequency centering and pulse width (P90 and P180). Following instrument calibration, standard oil samples of 0.00, 0.02, 0.05, and 0.20 g weight were used for calibration to establish signal response linearity and ensure measurement reproducibility.

The T_2 spectra of shale samples reflect how the oil-bearing porosity changes with relaxation time (Gao and Li, 2015; Li et al., 2019a). The LF-NMR signal strength (i.e., amplitude) is derived from the integration of the T_2 relaxation time distribution, and this amplitude represents the shale oil content (Tian et al., 2024). Continuous monitoring of the LF-NMR signal variations of the shale with time, it is possible to calculate the proportion and rate of shale oil loss, as follows:

$$\text{Loss proportion}_n = \frac{\text{Amplitude}_{\text{first}} - \text{Amplitude}_n}{\text{Amplitude}_{\text{first}}}, \quad (1)$$

where $\text{Amplitude}_{\text{first}}$ represents the first signal amplitude after completing the thermal simulation experiment. n denotes the exposure duration (in minutes) under ambient conditions, where Amplitude_n represents the LF-NMR signal amplitude corresponding to the n exposure interval. All amplitudes were normalized to sample mass and expressed in arbitrary units per gram, a.u./g.

The rate of shale oil loss indicates how quickly the shale oil is lost over time. The rate is defined as the temporal derivative of evaporative loss between consecutive exposure intervals ($n + 1$ and n), which can be quantified by the regression slope of the shale oil loss versus time. The EOM content losses occur during sampling, transportation, and time waiting for analysis and conducting experimental procedures. Consequently, the EOM represents the residual oil content after the maximum loss of shale oil, with its corresponding LF-NMR signal reflecting the stabilized hydrocarbon content at the terminal stage of measurable evaporative processes. The T_2 exhibits a linear correlation with shale pore size, as established by prior studies (Xu et al., 2015; Zhang et al., 2018; Li et al., 2019a):

$$d = C \times T_2, \quad (2)$$

where d is the pore diameter, nm; T_2 represents the transverse relaxation time, ms; and C denotes the calibration coefficient for unit conversion.

When calculating the pore size of shale using Eq. (2), the C value varies (Matteson et al., 2000; Zhang et al., 2018; Tian et al., 2020). In this study, the C value was corrected based on pore sizes obtained from low-temperature N_2 adsorption experiments.

2.2.3. Organic geochemical analysis

The TOC contents were measured with a LECO CS-230 instrument. Samples were pulverized to 200-mesh and washed with hydrochloric acid ($HCl:H_2O = 1:7$ by volume) at 60–80 °C for 1 h to remove carbonates. All the samples were then rinsed with distilled water to remove any remaining HCl and water-soluble chlorides. The samples were then dehydrated in a vacuum oven at 80 °C for 4 h. Subsequently, the samples were placed in an oxidation furnace at 850 °C, which has an infrared light detector. Organic carbon was combusted in a high-temperature stream of O_2, converting it to CO_2, which was then measured with the infrared detector.

Soxhlet extraction was conducted using dichloromethane (DCM) as a solvent and by refluxing at 85 °C for 72 h, which yielded EOM and a solid residue. To quantitatively characterize the hydrocarbon components, aliquots of 1 mL of DCM solution were analyzed with a HP-7890 GC instrument. The capillary column used for the GC was a HP-1 elastic silica capillary column (30 m long, 0.25 mm inner diameter, and 0.25 μm film thickness), with high-purity N_2 (N_2, 99.999%) used as the carrier gas at a constant flow rate of 1 mL/min. The GC oven temperature was initially held at 80 °C for 5 min, increased to 310 °C at a rate of 6 °C/min, and then maintained at that temperature for 35 min.

2.2.4. N_2 gas adsorption analysis

The N_2 adsorption analyses were performed using a Micromeritics ASAP 2020 surface area analyzer. Before measurement, approximately 300 mg of powdered samples were degassed under a vacuum chamber at 150 °C for 6 h to eliminate any residual gas impurities. N_2 adsorption isotherms were acquired at 77.35 K to detect mesopores (diameter = 2–50 nm) and macropores (diameter = 50–300 nm) (Clarkson et al., 2013). The adsorption-desorption measurements spanned a relative pressure (P/P_0) range of 0.005–0.998, where P represents equilibrium pressure and P_0 denotes the saturation pressure. Each pressure point maintained a 30-s equilibrium interval to ensure thermodynamic stability. The pore size distributions were derived from the adsorption branch using the Barrett-Joyner-Halenda (BJH) method with the Harkins-Jura thickness equation (Barrett et al., 1951).

3. Results and discussion

3.1. Geochemical characteristics of the shales

The TOC contents of the shale samples decreased progressively with increasing thermal maturity (Fig. 3(a)). The ratio of light to heavy components in the shale oil (C_6–C_{14}/C_{15+}) increased significantly at higher maturities (Fig. 3(b)). As the maturity increased, the hydrocarbon generation from the shale intensified, leading to a reduction in TOC contents from 3.20 wt% to 1.86 wt% (Fig. 3(a)). At thermal maturity levels below R_o = 1.2%, the shale is in the oil generation stage, generates mainly heavier hydrocarbons, and may have a relatively high oil adsorption capacity and a low free hydrocarbon content (Jarvie, 2012). During this stage, the C_6–C_{14}/C_{15+} ratio remains relatively constant (0.27–0.45). As R_o increases from 1.20% to 1.75%, gas becomes the primary hydrocarbon component because of thermal cracking of crude oil, with heavier components breaking down into lighter hydrocarbons. This results in a marked increase in the C_6–C_{14}/C_{15+} ratio, and the generated hydrocarbons become progressively lighter with increasing maturity (Fig. 3(b)).

3.2. Proportion and rate of shale oil loss

The temporal variations in the LF-NMR spectra of shale exposed to open air are primarily attributed to hydrocarbon evaporative loss. Although various experimental methods have been employed to investigate shale oil loss, including EOM gas chromatography (Song et al., 2013; Xue et al., 2016), Rock-Eval pyrolysis (Zhu et al., 2015; Jiang et al., 2016; Chen et al., 2017, 2018), mass balance methods (Chen et al., 2018), and chemical kinetic theory (Chen et al., 2017). Conventional destructive experimental methods, such as Rock-Eval pyrolysis and EOM analysis, require sample preparation (e.g., crushing), which can lead to underestimation of the shale oil content. Nuclear magnetic resonance (NMR) was used

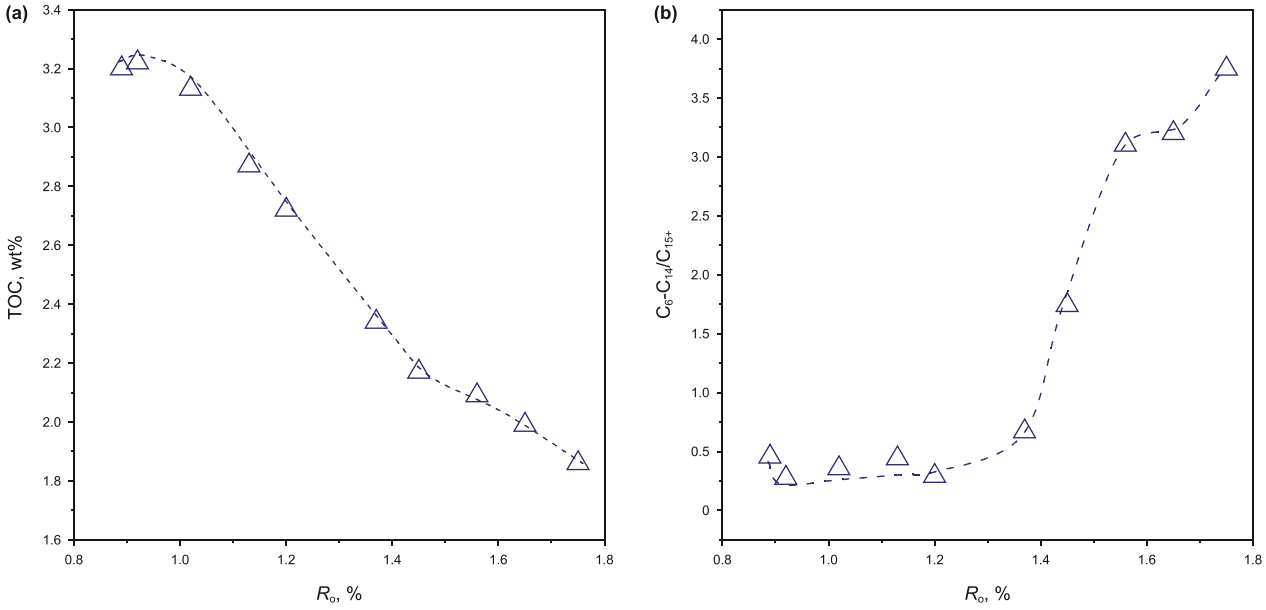

Fig. 3. Variations in the geochemical characteristics of the Qingshankou Formation shale samples with thermal maturity. (**a**) R_o (%) vs. TOC contents (wt%); (**b**) R_o (%) vs. light-to-heavy hydrocarbon ratio (C_6–C_{14}/C_{15+} ratio).

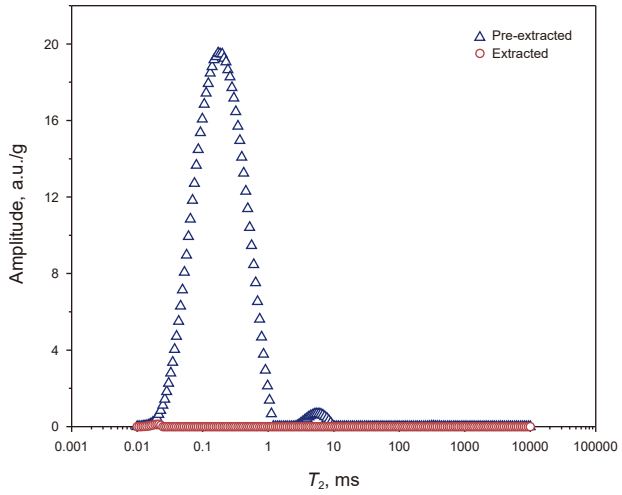

Fig. 4. Comparison of pre-extracted and extracted Shale LF-NMR T_2 Spectra (R_o = 0.92%).

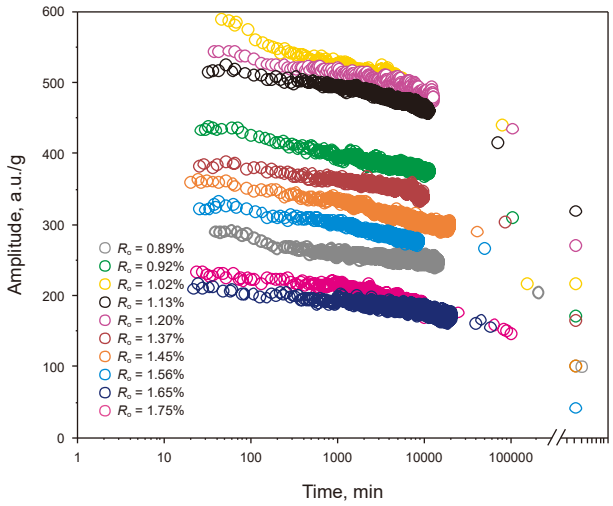

Fig. 5. Temporal variations of normalized LF-NMR signal amplitude (a.u./g) for Qingshankou Formation shales under atmospheric exposure.
Note: the terminal data points correspond to normalized LF-NMR signal amplitudes of EOM quantified in equivalent thermal maturity intervals (R_o = 0.89%–1.75%).

under low magnetic field to characterize unconventional shale oil and gas, including the shale fluid content, pore size distribution, and fluid occurrence state (Yao and Liu, 2012; Yao et al., 2014; Zhang et al., 2017; Li et al., 2019a; Song and Kausik, 2019; Bai et al., 2023; Zhao et al., 2023; Tian et al., 2024). Since NMR is sensitive to hydrogen-bearing fluids in porous media (Bloembergen et al., 1948; Coates et al., 1999; Meng et al., 2024), its direct measurement of shale oil content provides a more accurate determination of initial shale oil content (Gao and Li, 2015; Zhang et al., 2018; Song and Kausik, 2019; Bai et al., 2023; Meng et al., 2023). The previous studies have suggested the LF-NMR signal is affected by TOC content and clay minerals in the shale (Kausik et al., 2016; Li et al., 2019a). However, in this study, by comparing the LF-NMR signal intensity of the shale samples before and after extraction (Fig. 4), it was observed that the LF-NMR signal of the solid residue after extraction was nearly zero. This indicates the LF-NMR T_2 spectrum exclusively detects signals from hydrocarbons, with negligible interference from solid matrix components.

The normalized LF-NMR signal amplitude (expressed in a.u./g) of shales with varying thermal maturities exhibited a progressive decline with increasing exposure time (Fig. 5). With exposure time increased, the normalized LF-NMR amplitude demonstrated sustained attenuation, even after 1000 h (17 days) of exposure, the amplitude was persistent signal attenuation (Fig. 5). Initial amplitude values exhibited significant maturity-dependent variations (Fig. 5). Within the thermal maturity range from 0.89% to 0.92%, the first LF-NMR signal amplitudes ranged from 291 a.u./g to 434 a.u./g. Prolonged atmospheric exposure (> 1000 h) induced signal amplitude attenuation, resulting in amplitude reduction to

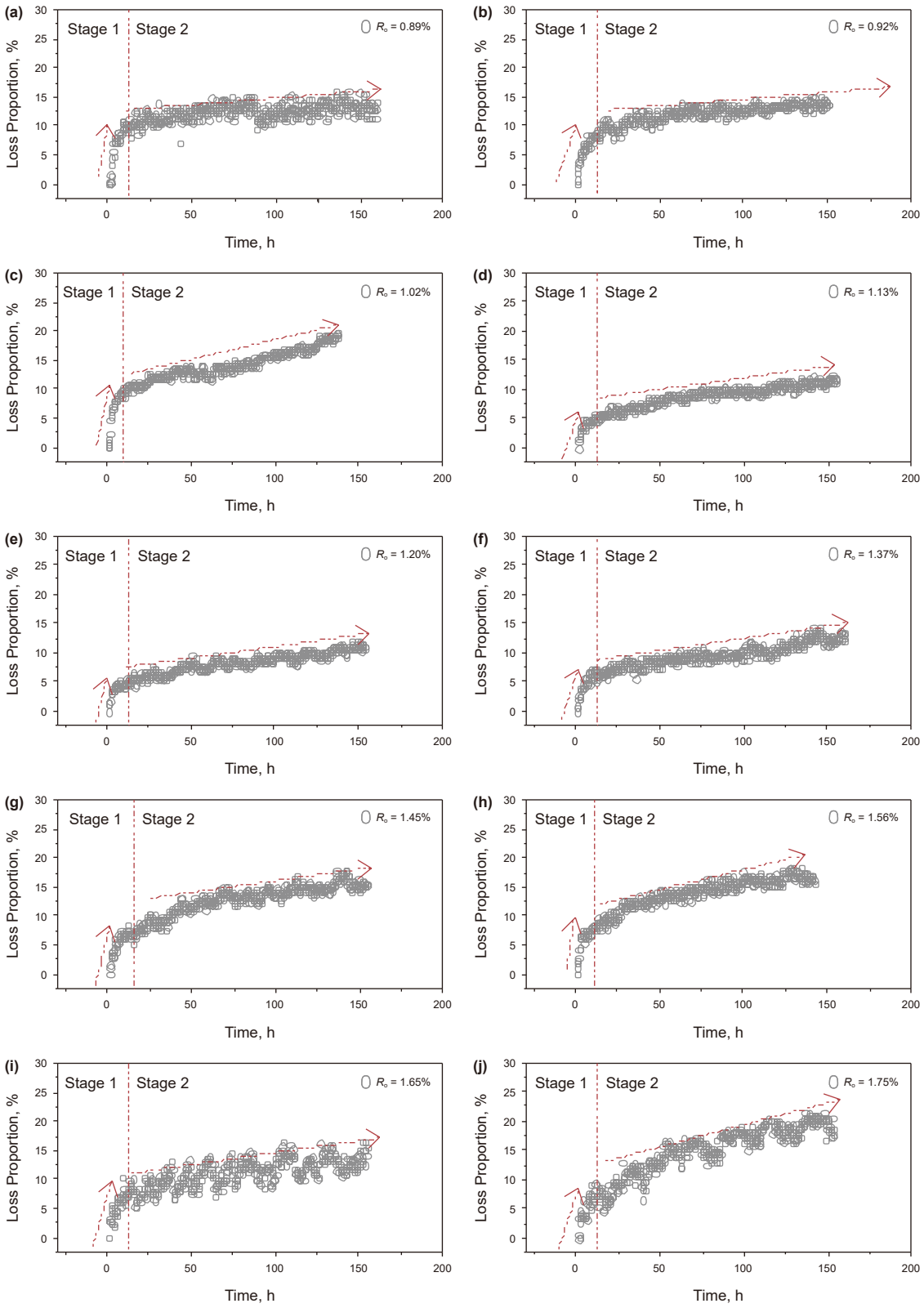

Fig. 6. Proportion of shale oil loss from the Qingshankou Formation shale samples with varying exposure times.

205–311 a.u./g. Within the early oil window (R_o = 1.02%–1.20%), shales exhibited the highest LF-NMR signal amplitudes (515–590 a.u./g), corresponding to peak oil generation observed across the thermal maturity range in this study. After > 1000 h of exposure in open air, the amplitudes decreased to 441, 436, and 416 a.u./g, respectively. Within the R_o = 1.37%–1.56%, Shale samples exhibited the first LF-NMR signal amplitudes were 384, 360, and 323 a.u./g, respectively. Prolonged atmospheric exposure (> 1000 h) induced signal attenuation, with amplitudes declining to 311, 304, and 268 a.u./g, respectively. For overmature shale samples (R_o = 1.65% and

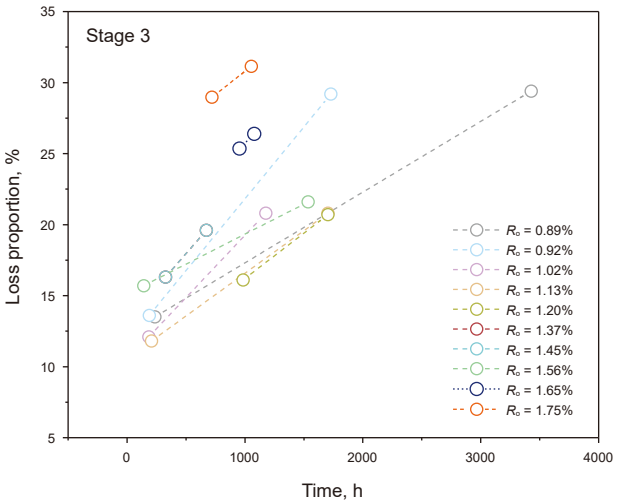

Fig. 7. Proportion of shale oil loss from the Qingshankou Formation shale samples with varying exposure times during stage 3.

Table 3
Rate of shale oil loss for the Qingshankou Formation shale samples with varying exposure times.

R_o	Loss rate, %		
	0~10 (hours)	10~150 (hours)	150~> 1000 (hours)
0.89	1.268	0.020	0.005
0.92	1.184	0.029	0.010
1.02	1.589	0.061	0.009
1.13	1.283	0.037	0.006
1.20	0.960	0.032	0.006
1.37	1.211	0.039	0.010
1.45	1.620	0.033	0.010
1.56	1.973	0.061	0.003
1.65	1.777	0.038	0.008
1.75	1.417	0.083	0.006

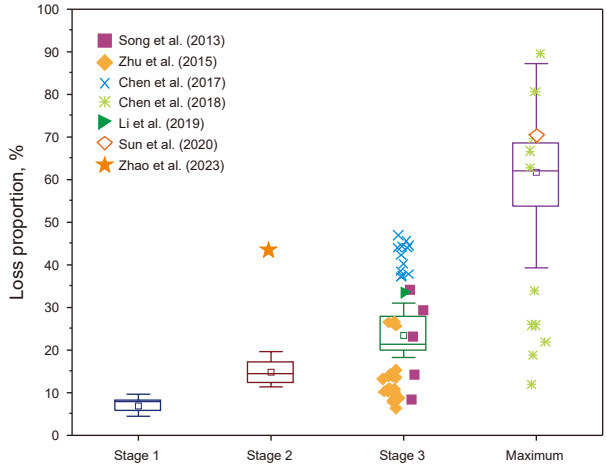

Fig. 8. Shale oil loss from the Qingshankou Formation shale samples during different stages, compared with results from previous studies (Song et al., 2013; Zhu et al., 2015; Chen et al., 2017, 2018; Li et al., 2019b; Sun, 2020; Zhao et al., 2023).

1.75%), the first LF-NMR signal amplitudes were 210 and 234 a.u./g, respectively. After > 1000 h of exposure under ambient conditions, the amplitudes decreased to 161 and 147 a.u./g, respectively.

Eq. (1) was used to calculate the proportion of shale oil loss at different exposure times (Figs. 6 and 7). The evaporative loss of shale oil can be divided into three stages, corresponding to the exposure times: (1) stage 1 occurs during the first 10 h, representing core recovery to the surface at the well site; (2) stage 2 occurs during 10–150 h, corresponding the transportation of samples from the well site to the laboratory, followed by short-term storage in the laboratory; and (3) stage 3 occurs during 150 h to > 1000 h, representing long-term storage of the samples in a core facility (Fig. 7).

During these three stages of shale oil loss, the proportion of loss increases gradually and the rate of loss shows a decrease (Table 3). In stage 1, the cumulative loss proportion of shale oil ranges from 0 to 10.9%, with a maximum loss rate of 1.250%/h (range: 0.183%/h–1.973%/h). Notably, previous studies have overlooked shale oil loss in stage 1, including those employing special coring techniques (e.g., pressurized, sponge-lined, and closed coring).

In stage 2, the cumulative loss proportion of shale oil ranges from 8.0% to 25.0%, with an average loss rate of 0.047%/h (range: 0.020%/h–0.097%/h), while stage 3 exhibits the shale oil losses of 19.5%–31.1%, with an average loss rate of 0.007%/h (0.003%/h–0.011%/h). There is no clear boundary between stages 2 and 3. Shale oil losses continue to occur when samples are not analyzed promptly after being transported from the well site to the laboratory, or stored for a long time in the core facility under ambient conditions. For example, the Devonian Duvernay Formation shale was exposed for 2 years before such a shale oil loss investigation, subsequent powdering, exhibited 37.5% hydrocarbon loss following pulverization and 21 h of exposure under ambient conditions (Jiang et al., 2016).

In previous research on shale oil evaporative loss, samples were routinely subjected to long-term storage in a core facility before analysis (Song et al., 2013; Zhu et al., 2015; Chen et al., 2017), and they also employed the chemical kinetic theory and the mass balance method to estimate the maximum evaporative loss proportion of shale oil (Chen et al., 2017, 2018). However, the previous studies of shale oil evaporative loss overlooked two critical stages: the original core recovery at the well site and sample transportation from the well site to the laboratory. By integrating results from the present investigation and previous research, a comprehensive schematic diagram was established to quantify evaporative losses, which can be accomplished by four key stages: stage 1: initial core retrieval at the well site; stage 2: the evaporative loss of shale oil due to exposure during its transportation from the well site to the laboratory; stage 3: long-time storage in a core facility; and stage 4: the maximum evaporative loss proportion of shale oil under ambient conditions. (Song et al., 2013; Zhu et al., 2015; Chen et al., 2017, 2018; Li et al., 2019b; Sun et al., 2020; Zhao et al., 2023) (Fig. 8). Shale oil loss in stage 1 ranges from 1% to 10%. This loss is typically overlooked, even with the application of sealed coring methods, and should be considered when assessing the original shale oil content. The shale oil loss in stage 2 ranges from 12% to 20%, with some samples losing as much as 43%. In stage 3, the total loss increases further and varies from 9% to 47%. The EOM extracted from shale represents the minimum value of the shale oil content, with its LF-NMR signal correspondingly minimized in shale samples. Under the assumption that artificial thermal simulation conditions maintain 100% oil retention, the maximum loss proportion of shale oil is calculated as the difference between the theoretical total oil content and the LF-NMR amplitude signal of EOM. Based on this assumption, the maximum loss proportion of shale oil in this study ranges from 39% to 87%. When integrating the previous studies (Chen et al., 2017, 2018), the maximum loss proportion of shale oil should range from 11% to 87%.

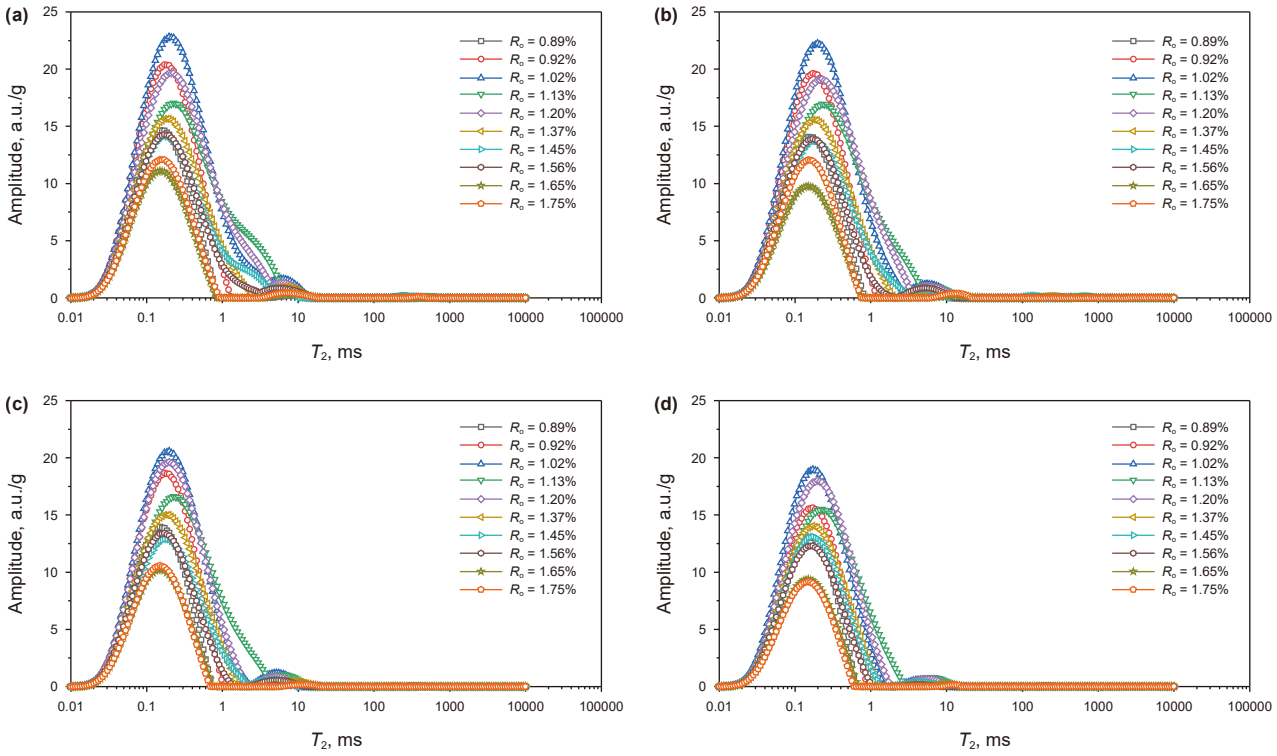

Fig. 9. LF-NMR signal amplitude per gram of rock for the Qingshankou Formation shale samples with increasing maturity at different exposure times. (**a**) 40 min; (**b**) 10 h; (**c**) 150 h; (**d**) > 1000 h.

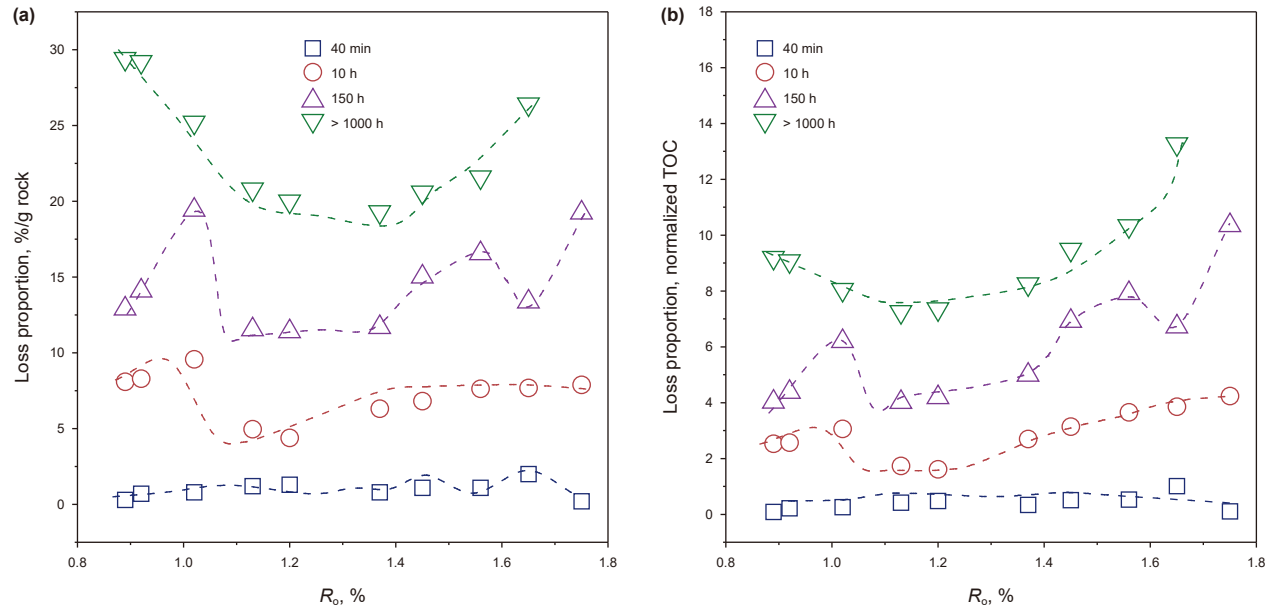

Fig. 10. Relationship between shale oil loss of the Qingshankou Formation shale samples, R_o values (thermal maturity), and exposure time. (**a**) R_o (%) vs. Loss proportion (%/g rock); (**b**) R_o (%) vs. Loss proportion (normalized TOC).

3.3. Factors controlling the evaporative loss of shale oil during thermal evolution

The LF-NMR T_2 spectra of the Qingshankou Formation shale samples (per gram of rock) exhibit progressive shifts under varying exposure durations, indicating dynamic equilibration of hydrocarbon loss processes with thermal evolution (Fig. 9). After reaching equilibrium, the shale oil loss initially decreases and then increases with maturity (Fig. 10(a)). At the initial state (exposure time $\leq$ 40 min), the shale oil loss is not significantly related to the degree of thermal evolution. As exposure time reaches *ca.* 10 h, the proportion of loss is in a dynamic loss state. After an exposure time of > 1000 h, the proportion of loss stabilizes and, as the thermal maturity increases from R_o = 0.89%–1.20%, the proportion of loss

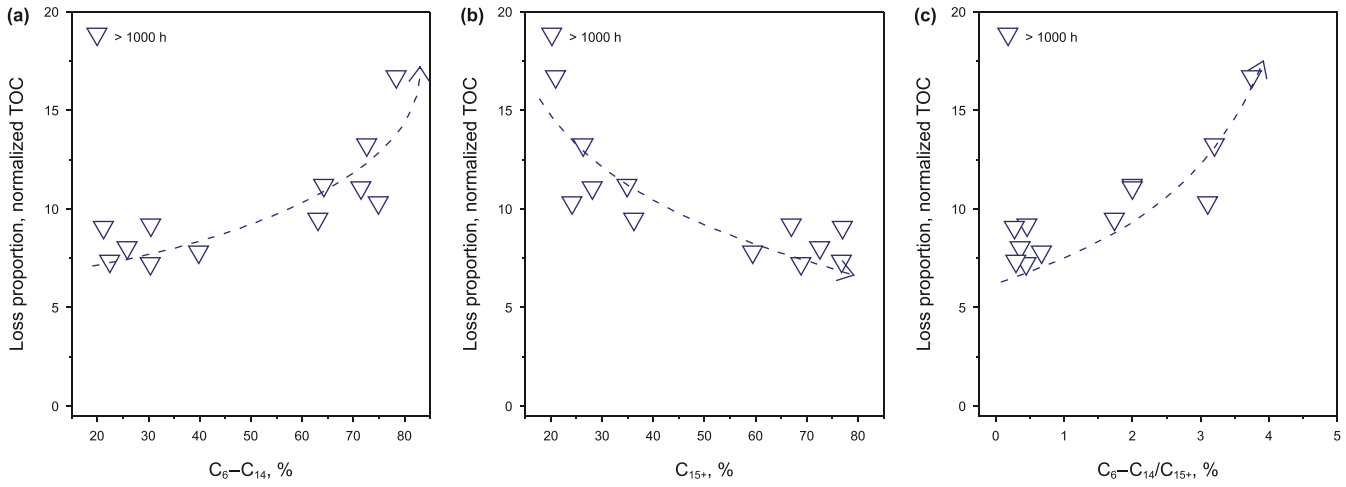

Fig. 11. Relationship between hydrocarbon composition and shale oil loss from the Qingshankou Formation shale samples. (**a**) C_6–C_{14} (%) vs. Loss proportion (normalized TOC); (**b**) C_{15+} (%) vs. Loss proportion (normalized TOC); (**c**) C_6–C_{14}/C_{15+} (%) vs. Loss proportion (normalized TOC).

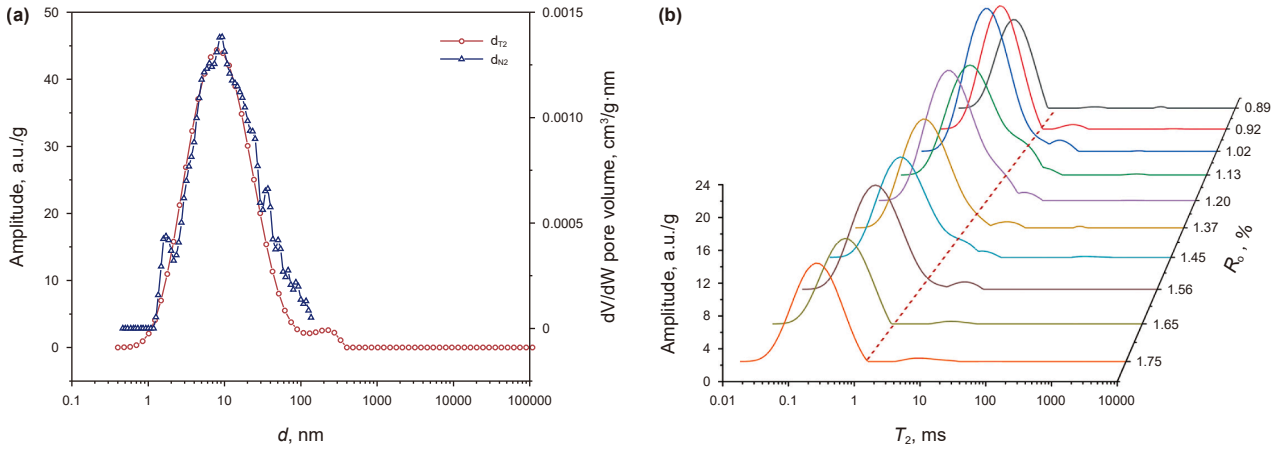

Fig. 12. Pore diameter distribution of the Qingshankou Formation shale samples, as characterized by LF-NMR T_2 spectra. (**a**) Pore diameters obtained from N_2 adsorption experiments and LF-NMR T_2 spectra (R_o = 0.92%). (**b**) LF-NMR T_2 spectra of the Qingshankou Formation shale samples.

decreases from 29.4% to 20.0%. However, as the maturity increases from R_o = 1.20%–1.75%, the shale oil loss increases from 20.0% to 31.1%, with a minimum loss at R_o = 1.20% (Fig. 10(a)).

Shale oil evaporative loss during thermal evolution is governed by three key factors: TOC, hydrocarbon composition, and pore size. By comparing the proportion of shale oil loss per unit rock weight and normalized to TOC content, we found that as the TOC content increases, the loss also increases (Fig. 10(a) and (b)). The effect of TOC on shale oil loss depends on the adsorption capacity of the shale samples, as well as the proportion of free oil. The hydrocarbon adsorption capacity per unit TOC mass is constant, implying that higher oil adsorption by the TOC results in greater saturation, making the hydrocarbons more prone to evaporation. For samples with very low oil saturation, if the TOC is in an undersaturated adsorption state, a high TOC content may reduce the shale oil loss (Jiang et al., 2016). Under favorable geological conditions for shale oil exploration and development, TOC content is in a saturated adsorption state with abundant free hydrocarbons. As the TOC content increases, the amount of free oil in the shale also increases (Lu et al., 2012; Wang et al., 2019), amplifying shale oil loss increased with higher TOC contents.

To further investigate the effects of hydrocarbon composition and pore size on hydrocarbon loss during thermal evolution, we conducted TOC-normalized loss quantification (Fig. 10(b)). When the hydrocarbon loss approaches a steady state, the loss first decreases and then increases with maturity, averaging 9.85% (range: 7.25%–16.72%). When R_o = 1.75%, the loss reaches a maximum of 16.72% (Fig. 10(b)).

The hydrocarbon composition is closely related to the proportion of shale oil loss, particularly the C_6–C_{14}/C_{15+} ratio of the liquid hydrocarbons. In the different maturity shale samples, as the proportion of C_6–C_{14} in the hydrocarbon components increases, the shale oil loss also increases (Fig. 11(a)). Conversely, as the proportion of C_{15+} in the hydrocarbon components increases, the shale oil loss decreases (Fig. 11(b)). As the C_6–C_{14}/C_{15+} ratio of the liquid hydrocarbons increases, the shale oil loss also increases (Fig. 11(c)), indicating the hydrocarbon composition plays a substantial role in the shale oil loss. The various components in the hydrocarbons have different parameters, such as polarity, molecular weight, and boiling temperature. Based on the stage state of the components, at a given temperature the lighter components have a higher saturated vapor pressure, making these easier to evaporate and leading to their faster loss. The lighter components preferential evaporate due to higher vapor pressures, establishing a chemical potential gradient that subsequently drives the sequential loss of heavier components. During short-term

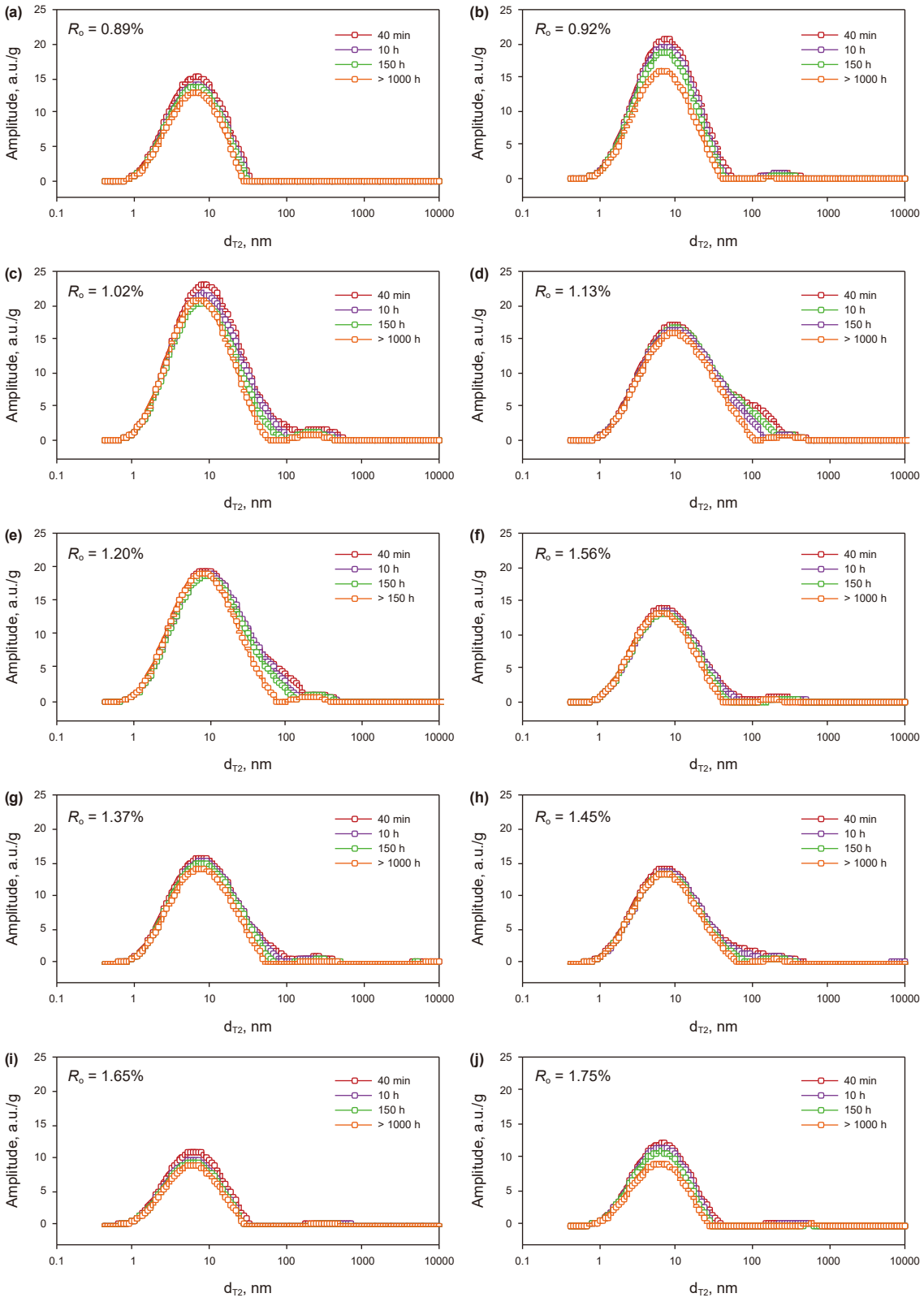

Fig. 13. Changes in oil-bearing pore diameter with exposure time for the Qingshankou Formation shale samples with different maturities.

exposure ($\leq$ 10 h), both the light (C_6–C_{14}) and heavy (C_{15+}) components undergo evaporative loss, driving maximal loss rates in stage 1. With prolonged exposure, depletion of light hydrocarbon fractions shifts mass transfer dominance to heavier components, whose lower evaporative loss kinetics, resulting in rate reductions during stages 2–3 compared to stages 1.

The analyzed shale samples exhibit a nanopore architecture dominated by small oil-bearing pores, as characterized by the LF-

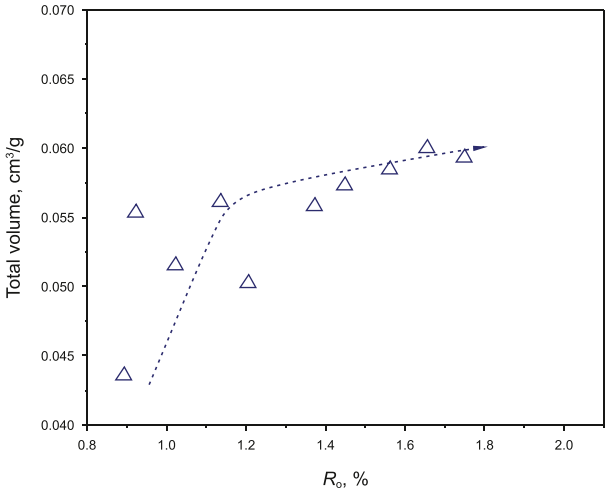

Fig. 14. Relationship between pore volume and shale oil loss for the Qingshankou Formation shale samples.

NMR T_2 spectra. Comparing T_2 relaxation-derived pore diameters (d_{T2}) with the N_2 adsorption data (d_{N2}), yielded an optimal scaling coefficient $C = 40$ for NMR-to-pore size conversion (Fig. 12(a)). A distinct peak and trough occur around the T_2 cutoff value of 2 ms, which effectively divide the entire spectrum into leading and trailing peaks (Fig. 12(b)). The pore diameter range for the leading peak is 0.4–80 nm, and for the trailing peak is 80–1000 nm. Based on the International Union of Pure and Applied Chemistry (IUPAC) classification, nanopores are divided into micropores (pore diameter < 2 nm), mesopores (pore diameter = 2–50 nm), and macropores (pore diameter > 50 nm) (Sing, 1985). The leading peak represents mesopores, while the trailing peak represents macropores.

The LF-NMR T_2 spectra of the shale samples vary with exposure time, revealing differential hydrocarbon evaporative loss with variable pore diameters (Fig. 13). Macropores exhibit rapid hydrocarbon losses, whereas mesopores dominate cumulative loss proportion despite slower loss rates. Following prolonged exposure (> 1000 h), T_2 spectra of the different thermal maturity samples display almost no amplitude signal beyond 2 ms

Table 4
Correlations between TOC content, pore volume, C_6–C_{14}/C_{15+} ratio, and shale oil loss at different maturities.

		Loss proportion (per rock)	
		R_o 0.89%–1.20%	R_o 1.20%–1.75%
TOC	Pearson correlation	0.957[a]	−0.267
	significant (2 tailed)	0.011	0.562
Pore volume	Pearson correlation	−0.289	0.005
	significant (2 tailed)	0.637	0.992
C_6–C_{14}/C_{15+}	Pearson correlation	0.053	0.851[a]
	significant (2 tailed)	0.933	0.015

[a] = Correlation is significant at the 0.05 level (two-tailed distribution).

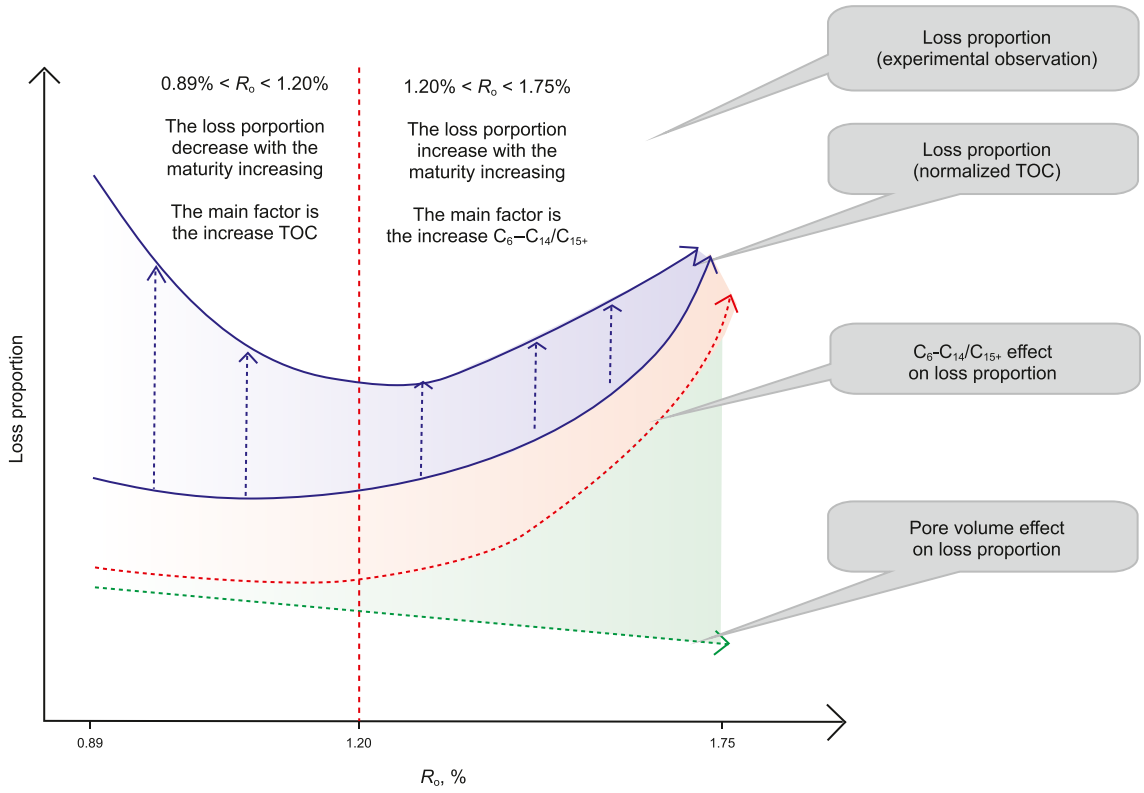

Fig. 15. Model of the factors that affect shale oil loss.

(Fig. 12(b)), indicating the hydrocarbons in macropores have been completely lost. In contrast, the amplitude signal from the small pores decreases more significantly with exposure time, and the absolute loss from the mesopores increases with exposure time. Zhao et al. (2023) quantified the shale oil loss of the Paleogene Ganchaigou Formation in the Qaidam Basin employing an analogous LF-NMR T_2 spectral analysis technique. After 43 h of pressurized coring, the shale oil loss was 43%, which closely aligned with Stage 2 losses in this study. The LF-NMR T_2 spectrum signal of the Ganchaigou Formation shales ranged from 2 to 10 ms, and significantly longer than those of the studied shale samples. Therefore, the hydrocarbons in large pores were preferentially lost, which explains why the shale oil loss from the Ganchaigou Formation exceeds that in the second stage of the present study.

Organic matter generates organic-hosted nanopores during hydrocarbon generation during the thermal maturity (R_o = 0.89%–1.75%) (Curtis et al., 2012; Wang et al., 2024), with total pore volume increasing from 0.04 to 0.06 cm^3/g (Fig. 14). The increase in nanopores enhanced the shale oil adsorption, resulting in a decrease in shale oil loss. From R_o = 0.89%–1.20%, the nanopores grew rapidly, reducing shale oil loss. However, from R_o = 1.20%–1.75%, the nanopore shows little significant change. This result contradicts the previous assumptions that an increase in nanopores leads to a constant decrease in shale oil loss (Jiang et al., 2016; Chen et al., 2018).

Based on our findings, we developed a comprehensive model identifying the key controls for shale oil loss (Fig. 15). During the low to medium maturity stages (R_o = 0.89%–1.20%), the shale oil loss decreases with increasing maturity, which is due primarily to the decrease in TOC content. The correlations between shale oil loss, TOC content, hydrocarbon composition, and pore volume indicate that TOC content has the strongest correlation with shale oil loss (Table 4). An increase in pore volume contributes to a decrease in the shale oil loss. Previous studies attributed the decrease in shale oil loss to the increasing density of shale oil at greater burial depths in the low to medium maturity stages (Chen et al., 2018). However, the present study used shale samples from laboratory thermal simulation, which effectively eliminates the effect of shale heterogeneity on shale oil loss. Therefore, the shale oil loss in these maturity stages is affected primarily by TOC content, with the hydrocarbon composition and pore volume acting as secondary factors.

In the medium to high maturity stages (R_o = 1.20%–1.75%), the shale oil loss increases with maturity, driven primarily by an increase in the C_6–C_{14}/C_{15+} ratio of the hydrocarbons (Table 4); the changes in pore volume and TOC content are less important.

4. Conclusions and indication

Through the thermal simulation experiments on low-maturity shale samples from the Qingshankou Formation in the Songliao Basin, we obtained the T_2 spectra variation of the shale samples, and quantified both the temporal proportion and rate of shale oil loss with maturities ranging from 0.89% to 1.75% using LF-NMR. The temporal evolution trends and controlling factors of shale oil loss were systematically investigated. The main conclusions are as follows:

The TOC content, hydrocarbon C_6–C_{14}/C_{15+} ratios, and shale oil loss exhibit significant variations across thermal evolution stages. With increasing thermal maturity (R_o = 0.89%–1.75%), the TOC content of the shales decreases from 3.20% to 1.86%. The hydrocarbon C_6–C_{14}/C_{15+} ratios remained stable during early maturation (R_o = 0.89%–1.20%), whereas beyond the peak of hydrocarbon generation (R_o > 1.20%), it increased rapidly from 0.29% to 3.75%.The shale oil loss decreases with increasing maturity at the low to medium maturity stages (R_o = 0.89%–1.20%), and this decrease in shale oil loss is due to the decrease in TOC contents, not the previous results of shale oil density increasing. While the shale oil loss increases with maturity at the medium to high maturity stages (R_o = 1.20%–1.75%), the hydrocarbon composition changing (i.e., an increase in C_6–C_{14}/C_{15+} ratios), is the main factor that causes the increase in shale oil loss rather than TOC content.

Based on the variations in the proportion and rate of shale oil loss for the different shales and exposure times, the evaporative loss of shale oil can be divided into three stages, stage 1 involves a shale oil loss of 0–10.9% (during the first 10 h after core recovery to the surface at the well site), stage 2 involves a shale oil loss of 8.0%–25.0%, and stage 3 involves a shale oil loss of 19.5%–31.1%. So, with increasing exposure time of the shale samples, the shale oil content of the different thermal maturity samples decreased continuously.

The highest proportion of shale oil loss occurred shortly after drilling (< 10 h), reaching approximately 10% of total oil content. Delayed analysis of shale samples after drilling may lead to significant evaporative loss, with maximum proportion of losses ranging from 11% to 89%. The proportion of shale oil loss is different during the following three stages, the first 10 h during the transfer of the shale from its in-situ reservoir to the surface at the well site, the second 150 h of transportation of the shale from the well site to the laboratory, including sorting, packaging, and transport, and last more than 1000 h of storage of samples. Therefore, we should pay more attention to this hydrocarbon evaporative loss at different stages in future shale oil resource assessments.

CRediT authorship contribution statement

Xue-Ning Qi: Methodology, Investigation, Writing – original draft, Conceptualization, Writing – review & editing. **Hua Tian:** Funding acquisition, Writing – review & editing, Methodology. **Xiao-Mei Wang:** Supervision, Funding acquisition, Writing – review & editing. **Ming-Hao Wu:** Writing – original draft. **Yu-Ke Liu:** Visualization. **Shui-Chang Zhang:** Writing – review & editing, Resources.

Declaration of competing interest

The authors declare that they have no known competing financial interests or personal relationships that could have appeared to influence the work reported in this paper.

Acknowledgements

This work was supported by the National Natural Science Foundation of China (Grants U22B6004) and PetroChina R&D Program (Grants 2021DJ0104, 2022-KFKT-09).

References

Abrams, M.A., Gong, C., Garnier, C., et al., 2017. A new thermal extraction protocol to evaluate liquid rich unconventional oil in place and in-situ fluid chemistry. Mar. Petrol. Geol. 88, 659–675. https://doi.org/10.1016/j.marpetgeo.2017.09.014.

Akkutlu, I.Y., 2017. Shale resource assessment in presence of nanopore confinement. In: Proceedings of the 5th Unconventional Resources Technology Conference. American Association of Petroleum Geologists, Austin, Texas, USA. https://doi.org/10.15530/URTEC-2017-2670808.

Bai, L.H., Liu, B., Fu, X.F., et al., 2023. A new method for evaluating the oil mobility based on the relationship between pore structure and state of oil. Geosci. Front. 14, 101684. https://doi.org/10.1016/j.gsf.2023.101684.

Barrett, E.P., Joyner, L.G., Halenda, P.P., 1951. The determination of pore volume and area distributions in porous substances. I. Computations from nitrogen isotherms. J. Am. Chem. Soc. 73, 373–380. https://doi.org/10.1021/ja01145a126.

Bloembergen, N., Purcell, E.M., Pound, R.V., 1948. Relaxation effects in nuclear magnetic resonance absorption. Phys. Rev. 73 (7), 679. https://doi.org/10.1103/PhysRev.73.679.
Chen, G.H., Lu, S.F., Zhang, J.F., et al., 2017. Estimation of enriched shale oil resource potential in E_2s_4L of Damintun sag in Bohai Bay Basin, China. Energy Fuel. 31, 3635–3642. https://doi.org/10.1021/acs.energyfuels.6b03201.
Chen, J.Q., Pang, X.Q., Pang, H., et al., 2018. Hydrocarbon evaporative loss evaluation of lacustrine shale oil based on mass balance method: Permian Lucaogou Formation in Jimusaer Depression, Junggar Basin. Mar. Petrol. Geol. 91, 422–431. https://doi.org/10.1016/j.marpetgeo.2018.01.021.
Clarkson, C.R., Solano, N., Bustin, R.M., et al., 2013. Pore structure characterization of North American shale gas reservoirs using USANS/SANS, gas adsorption, and mercury intrusion. Fuel 103, 606–616. https://doi.org/10.1016/j.fuel.2012.06.119.
Coates, G.R., Xiao, L., Prammer, M.G., 1999. NMR Logging: Principles and Applications. Halliburton Energy Services, Houston, Tex.
Curtis, M.E., Cardott, B.J., Sondergeld, C.H., et al., 2012. Development of organic porosity in the Woodford Shale with increasing thermal maturity. Int. J. Coal Geol. 103, 26–31. https://doi.org/10.1016/j.coal.2012.08.004.
Gao, H., Li, H.Z., 2015. Determination of movable fluid percentage and movable fluid porosity in ultra-low permeability sandstone using nuclear magnetic resonance (NMR) technique. J. Pet. Sci. Eng. 133, 258–267. https://doi.org/10.1016/j.petrol.2015.06.017.
Hong, Z.Q., Meng, M.M., Deng, K., et al., 2025. A quick method for appraising pore connectivity and ultimate imbibed porosity in shale reservoirs. J. Mar. Sci. Eng. 13 (1), 174. https://doi.org/10.3390/jmse13010174.
Hopkins, A.S., 2017. The next energy economy. Science 356, 709. https://doi.org/10.1126/science.aam8696.
Hu, T., Pang, X.Q., Jiang, F.J., et al., 2021. Movable oil content evaluation of lacustrine organic-rich shales: Methods and a novel quantitative evaluation model. Earth Sci. Rev. 214, 103545. https://doi.org/10.1016/j.earscirev.2021.103545.
Hughes, J.D., 2013. A reality check on the shale revolution. Nature 494, 307–308. https://doi.org/10.1038/288688a0.
Jarvie, D.M., 2012. Shale resource systems for oil and gas: Part 2—Shale-oil resource systems shale reservoirs—giant resources for the 21st century. Amer Ass Pet. Geolo. Tulsa, 89–119.
Jarvie, D.M., Hill, R.J., Ruble, T.E., et al., 2007. Unconventional shale-gas systems: the Mississippian barnett shale of north-central Texas as one model for thermogenic shale-gas assessment. AAPG Bull. 91, 475–499. https://doi.org/10.1306/12190606068.
Jiang, C.J., Chen, Z.H., Mort, A., et al., 2016. Hydrocarbon evaporative loss from shale core samples as revealed by Rock-Eval and thermal desorption-gas chromatography analysis: Its geochemical and geological implications. Mar. Petrol. Geol. 70, 294–303. https://doi.org/10.1016/j.marpetgeo.2015.11.021.
Kausik, R., Fellah, K., Feng, L., et al., 2016. High- and low-field NMR relaxometry and diffusometry of the bakken petroleum system. SPWLA. https://go.exlibris.link/vlxZKs9.
Li, J.B., Lu, S.F., Jiang, C.Q., et al., 2019a. Characterization of shale pore size distribution by NMR considering the influence of shale skeleton signals. Energy Fuel. 33, 6361–6372. https://doi.org/10.1021/acs.energyfuels.9b01317.
Li, M.W., Chen, Z.H., Ma, X.X., et al., 2019b. Shale oil resource potential and oil mobility characteristics of the Eocene-Oligocene Shahejie Formation, Jiyang Super-Depression, Bohai Bay Basin of China. Int. J. Coal Geol. 204, 130–143. https://doi.org/10.1016/j.coal.2019.01.013.
Lu, S.F., H, W.B., C, F.W., et al., 2012. Classification and evaluation criteria of shale oil and gas resources: Discussion and application. Petrol. Explor. Dev. 39 (2), 268–276. https://doi.org/10.1016/S1876-3804(12)60042-1.
Luo, C., Zhang, H.X., Zhang, J.Z., et al., 2022. Evaluation of oil content in shale by sealed thermal desorption: A case study of Jurassic Da'an Zhai Member, Sichuan Basin. Pet. Geolo. Exp. 44, 712–718 (in Chinese). https://doi.org/10.11781/sysydz20224712.
Matteson, A., Tomanic, J.P., Herron, M.M., et al., 2000. NMR relaxation of clay/brine mixtures. SPE Reservoir Eval. Eng. 3 (5), 408–413. https://doi.org/10.2118/66185-PA.
Meng, M.M., Hu, Q.H., Wang, Q.Y., et al., 2024. Effect of initial water saturation and water film on imbibition behavior in tight reservoirs using nuclear magnetic resonance technique. Phys. Fluids 36 (5), 056603. https://doi.org/10.1063/5.0209910.
Meng, M.M., Zhang, Y.X., Yuan, B., et al., 2023. Imbibition behavior of oil-saturated rock: Implications for enhanced oil recovery in unconventional reservoirs. Energy Fuel. 37 (18), 13759–13768. https://doi.org/10.1021/acs.energyfuels.3c02501.
Mi, J.K., Zhang, S.C., Wang, X.M., et al., 2009. Comparison of different hydrocarbon generation simulation approaches and key technique. Pet. Geol. Exp. 31, 409–414 (in Chinese). https://doi.org/10.11781/sysydz200904409.
Michael, G.E., Packwood, J., Holba, A., 2013. Determination of in-situ hydrocarbon volumes in liquid rich shale plays. In: SPE/AAPG/SEG unconventional resources technology conference. https:doi.org/168695/URTeC1573030.
Milliken, K.L., Rudnicki, M., Awwiller, D.N., et al., 2013. Organic matter-hosted pore system, Marcellus Formation (Devonian), Pennsylvania. AAPG Bull. 97, 177–200. https://doi.org/10.1306/07231212048.
Şen, Ş., Kozlu, H., 2020. Impact of maturity on producible shale oil volumes in the Silurian (Llandovery) hot shales of the northern Arabian plate, southeastern Turkey. AAPG Bull. 104 (3), 507–524. https://doi.org/10.1306/05141917201.
Sing, K.S., 1985. Reporting physisorption data for gas/solid systems with special reference to the determination of surface area and porosity. Pure Appl. Chem. 57, 603–619. https://doi.org/10.1351/pac198557040603.
Song, G.Q., Lu, S.F., Xu, X.Y., et al., 2013. Resource evaluation method for shale oil and its application. Earth Sci. Front. 20, 221–228 (in Chinese).
Song, Y.Q., Kausik, R., 2019. NMR application in unconventional shale reservoirs—A new porous media research frontier. Prog. Nucl. Magn. Reson. Spectrosc. 112–113, 17–33. https://doi.org/10.1016/j.pnmrs.2019.03.002.
Sun, L.D., 2020. Gulong shale oil (preface). Pet. Geol. Oilfield Dev Daqing 39 (3), 1–7 (in Chinese). https://doi.org/10.19597/J.ISSN.1000-3754.202005037.
Sweeney, J.J., Burnham, A.K., 1990. Evaluation of a simple model of vitrinite reflectance based on chemical kinetics. AAPG Bull. 74, 1559–1570. https://doi.org/10.1306/0C9B251F-1710-11D7-8645000102C1865D.
Tian, H., He, K., Huangfu, Y.H., et al., 2024. Oil content and mobility in a shale reservoir in Songliao Basin, Northeast China: Insights from combined solvent extraction and NMR methods. Fuel 357, 129678. https://doi.org/10.1016/j.fuel.2021.121319.
Tian, H., Wang, M.Z., Liu, S.B., et al., 2020. Influence of pore water on the gas storage of organic-rich shale. Energy Fuel. 34 (5), 5293–5306. https://doi.org/10.1021/acs.energyfuels.9b03415.
Tian, L.J., Hu, G.Y., Guo, J.H., et al., 2023. New insight into abiotic or biotic gas in deep reservoirs of the CL-I gas field in Songliao Basin (China) by light hydrocarbons associated with natural gas. Mar. Petrol. Geol. 149, 106091. https://doi.org/10.1016/j.marpetgeo.2022.106091.
Wang, L., Liu, B., Bai, L.H., et al., 2024. Pore evolution modeling in natural lacustrine shale influenced by mineral composition: implications for shale oil exploration and CO_2 storage. Advances in Geo-Energy Research 13, 218–230. https://doi.org/10.46690/ager.2024.09.07.
Wang, M., Li, M., Li, J.B., et al., 2022. The key parameter of shale oil resource evaluation: Oil content. Pet. Sci. 19, 1443–1459. https://doi.org/10.1016/j.petsci.2022.03.006.
Wang, M., Guo, Z.Q., Jiao, C.X., et al., 2019. Exploration progress and geochemical features of lacustrine shale oils in China. J. Petrol. Sci. Eng. 178, 975–986. https://doi.org/10.1016/j.petrol.2019.04.029.
Xu, H., Tang, D.Z., Zhao, J.L., et al., 2015. A precise measurement method for shale porosity with low-field nuclear magnetic resonance: A case study of the Carboniferous–Permian strata in the Linxing area, eastern Ordos Basin, China. Fuel 143, 47–54. https://doi.org/10.1016/j.fuel.2014.11.034.
Xue, H.T., Tian, S.S., Wang, W.M., et al., 2016. Correction of oil content-one key parameter in shale oil resource assessment. Oil Gas Geol 37, 15–22 (in Chinese). https://doi.org/10.11743/ogg20160103.
Yan, G., Xu, Y.H., Xu, W.L., et al., 2023. Shale oil resource evaluation with an improved understanding of free hydrocarbons: insights from three-step hydrocarbon thermal desorption. Geosci. Front. 14, 101677. https://doi.org/10.1016/j.gsf.2023.101677.
Yan, J., Wang, W.Z., Zhang, H.C., et al., 2019. Practice of turbo-drill core drilling in Well SK-2. Drill. Prod. Technol. 42, 31–34 (in Chinese). https://doi.org/10.3969/J.ISSN.1006-768X.2019.01.10.
Yao, Y.B., Liu, D.M., 2012. Comparison of low-field NMR and mercury intrusion porosimetry in characterizing pore size distributions of coals. Fuel 95, 152–158. https://doi.org/10.1016/j.fuel.2011.12.039.
Yao, Y.B., Liu, D.M., Xie, S.B., 2014. Quantitative characterization of methane adsorption on coal using a low-field NMR relaxation method. Int. J. Coal Geol. 131, 32–40. https://doi.org/10.1016/j.coal.2014.06.001.
Zhang, P.F., Lu, S.F., Li, J.Q., et al., 2018. Petrophysical characterization of oil-bearing shales by low-field nuclear magnetic resonance (NMR). Mar. Petrol. Geol. 89, 775–785. https://doi.org/10.1016/j.marpetgeo.2017.11.015.
Zhang, P.F., Lu, S.F., Li, J.Q., et al., 2017. Characterization of shale pore system: A case study of Paleogene Xin'gouzui Formation in the Jianghan Basin, China. Mar. Petrol. Geol. 79, 321–334. https://doi.org/10.1016/j.marpetgeo.2016.10.014.
Zhao, W.Z., Zhu, R.K., Liu, W., et al., 2023. Advances in theory and technology of non-marine shale oil exploration in China. Petroleum Science Bulletin 4, 373–390. https://doi.org/10.3969/j.issn.2096-1693.2023.04.029.
Zhu, R.F., Zhang, L.Y., Li, J.Y., et al., 2015. Quantitative evaluation of residual liquid hydrocarbons in shale. Acta Pet. Sin. 36, 13–18 (in Chinese). https://doi.org/10.7623/syxb201501002.
Zou, C.N., Yang, Z., Cui, J.W., et al., 2013. Formation mechanism, geological characteristics and development strategy of nonmarine shale oil in China. Petrol. Explor. Dev. 40, 15–27. https://doi.org/10.1016/S1876-3804(13)60002-6.